Quantum Monte Carlo calculations of dark matter scattering off light nuclei

Lorenzo Andreoli, Vincenzo Cirigliano, Stefano Gandolfi, and Francesco Pederiva

Phys. Rev. C **99**, 025501 — Published 8 February 2019

DOI: 10.1103/PhysRevC.99.025501

Quantum Monte Carlo calculations of dark matter scattering off light nuclei

Lorenzo Andreoli,[1,2,3] Vincenzo Cirigliano,[1] Stefano Gandolfi,[1] and Francesco Pederiva[2,3]

[1] *Theoretical Division, Los Alamos National Laboratory, Los Alamos, New Mexico 87545, USA*
[2] *Dipartimento di Fisica, University of Trento, via Sommarive 14, I-38123 Povo, Trento, Italy*
[3] *INFN-TIFPA, Trento Institute for Fundamental Physics and Applications, 38123 Trento, Italy*

(Dated: January 28, 2019)

We compute the matrix elements for elastic scattering of dark matter (DM) particles off light nuclei (^{2}H, ^{3}H, ^{3}He, ^{4}He and ^{6}Li) using Quantum Monte Carlo Methods. We focus on scalar-mediated DM-nucleus interactions and use scalar currents obtained to next-to-leading order in chiral effective theory. The nuclear ground states are obtained from a phenomenological nuclear Hamiltonian that includes the Argonne v_{18} two-body interaction and the three-body Urbana IX. Within this approach, we study the impact of one- and two-body currents and discuss the size of nuclear uncertainties, including for the first time two-body effects in $A = 4, 6$ systems. Our results provide the nuclear structure input needed to assess the sensitivity of future experimental searches of (light) dark matter using light nuclei, such as ^{3}He and ^{4}He.

I. INTRODUCTION

Observational evidence for Dark Matter (DM) in the universe is extremely strong, coming both from astrophysics and cosmology [1]. While searches for signals from direct, indirect, and accelerator experiments have yet to be successful, a vibrant worldwide experimental program exists. In particular, the so-called "direct detection" search for weakly interacting massive particles (WIMPs) through nuclear recoils is very active, and there is a growing emphasis on covering a broader DM mass range, extending to the sub-GeV scale [2].

As emphasized already in early studies [3], in order to interpret direct detection experiments and disentangle the origin of possible future signals, it is important to have a solid theoretical control of nuclear effects. In recent years, a variety of approaches based on effective field theory (EFT) have been proposed to tackle the physics of DM-nucleus interactions. EFT methods have been applied at different levels: (i) non-relativistic DM-nucleus interactions [4]; (ii) non-relativistic DM-nucleon interactions [5]; (iii) DM-nucleon interactions derived from DM-quark and DM-gluon interactions in the framework of chiral-EFT [6–12], to be used in nuclear few- and many-body calculations. Firts principle, lattice-QCD calculations, have also been performed for matrix elements of scalar, axial, and tensor currents [13, 14].

We work within approach (iii), which is the only one suitable for matching to higher scales and performing a consistent phenomenology of direct, indirect, and collider DM searches. In this approach, several classes of operators arise at the DM-quark and DM-gluon level (see for example [12] and references therein). In this work, we focus on scalar-mediated DM-quark and DM-gluon interactions, which could, for example, arise from the exchange of particles from an extended Higgs sector in UV models. However, we emphasize that our nuclear matrix elements apply also to the case of "light" scalar mediators, with masses below the electroweak scale (the expression for the DM-nucleus scattering amplitude would have to be multiplied in that case by the appropriate light scalar propagator). The choice of scalar-mediated interactions for this exploratory study is motivated by the fact that two-nucleon currents arise in this case already at NLO in the chiral counting, while they are relatively more suppressed for other interactions [9].

We focus on DM scattering off a variety of light nuclei, namely ^{2}H, ^{3}H, ^{3}He, ^{4}He and ^{6}Li. Our study has a twofold motivation. First, for such light nuclei first-principles calculations of the nuclear wave functions are possible, once nucleon-level interactions are specified. Therefore one can reliably study the effect of one- and two-nucleon currents for different spin and isospin structures. Second, light nuclear targets are of great interest because they provide a better kinematic match for light DM and allow one to probe sub-GeV DM masses [2]. In fact, both ^{3}He and ^{4}He isotopes are being considered for future direct detection experiments [15–19], including directional detection [20]. So our study goes beyond the benchmarking scope and will be relevant in the interpretation of results from these experiments.

In our study we follow a hybrid approach in which the scalar-mediated DM-nucleon interactions are derived in the framework of chiral-EFT up to next-to-leading-order (NLO) in the Weinberg counting [7], and the nuclear wave functions are obtained from a phenomenological nuclear Hamiltonian than includes accurate two-body [21] and three-body interactions [22]. This allows us to take advantage of Quantum Monte Carlo methods, that in recent years have proven to be extremely successful in describing light and medium-heavy nuclei from first principles [23–25]. Within this framework, the impact of two-body currents has been previously studied in electron scattering [26, 27] and neutral-current neutrino scattering [27, 28] (finding effects up to O(10%)), as well as in β-decays [29] (finding effects of few %).

First-principles studies of DM-nucleus scattering for light nuclei already exist in the recent literature [11, 30]. Ref. [11] focuses on systems with A=2,3 and performs a self-consistent analysis of scalar-mediated DM-nucleus scattering using both chiral currents and chiral poten-

tials for the nuclear wave functions. Ref. [30], on the other hand, focuses on ^{3}He and ^{4}He isotopes and uses a hybrid approach (different from ours) in which nuclear wave functions are obtained in the no-core shell model with NNLO chiral potential while general one-body "currents" (not just scalar-mediated) are parametrized in the non-relativistic EFT framework of Ref. [5]. While overlapping with these studies, our work provides the first results for two-nucleon currents in systems with A=4,6, including the ^{4}He isotope of experimental interest.

The paper is organized as follows: we summarize the relevant scalar-mediated DM-nucleon interactions in Section II. In Section III we give the detail of nuclear Hamiltonian and wave functions used for the calculations of the elastic scattering cross section and in Section IV we present our results. We give our conclusions and outlook in Section V.

II. SCALAR INTERACTION

A general, model-independent interaction for DM and quarks can be built using higher dimension operators of the form (see for example Ref. [12])

$$\mathcal{O} = \bar{\chi}\Gamma_\chi \chi \bar{\psi}\Gamma_\psi \psi, \tag{1}$$

where $\Gamma_{\chi/\psi} \in \{\mathbb{1}, \gamma^5, \gamma^\mu, \gamma^\mu\gamma^5\}$ are Dirac bilinears, χ and $\bar{\chi}$ are the DM fields, and ψ and $\bar{\psi}$ the quark fields.

In this work, we will restrict ourselves to scalar interaction between a DM particle and standard model fields (vector and axial-vector interactions will be studied in future work). The DM particle is assumed to be a Dirac fermion of spin 1/2. The effective Lagrangian describing scalar-mediated DM-quark and DM-gluon interaction is built from dimension-7 operators [7]:

$$\mathcal{L}_{\text{eff}} = \frac{1}{\tilde{\Lambda}^3}\left(\sum_{q=u,d,s} c_q \bar{\chi}\chi m_q \bar{q}q + c_G \bar{\chi}\chi \alpha_s G^a_{\mu\nu} G^{\mu\nu}_a\right), \tag{2}$$

where the sum runs over the light quark fields q, α_s is the strong coupling constant and $G_{\mu\nu}$ is the gluon field strength tensor. We have introduced a new physics scale $\tilde{\Lambda}$ related to the mass of the mediator (or possibly a new interaction mechanism) and dimensionless Wilson coefficients c_q, c_G that parametrize the interaction. For convenience, we include the masses of the quarks m_q in the definition of the operators.

The derivation of the interaction at the nucleon level can be found in [7, 10, 11, 31]. The diagrams contributing at this order are shown in Fig. 1. Here we only summarize the resulting currents up to NLO, in the context of $SU(2)$ chiral perturbation theory [10, 11].

We assume the following convention for momenta,

$$N(\boldsymbol{p}_i) + \chi(\boldsymbol{k}) \to N(\boldsymbol{p}'_i) + \chi(\boldsymbol{k}'), \tag{3}$$

where $\boldsymbol{q} = \boldsymbol{k}' - \boldsymbol{k} = \boldsymbol{p}_i - \boldsymbol{p}'_i$ and $\boldsymbol{p}_i$, $\boldsymbol{k}$ ($\boldsymbol{p}'_i$, $\boldsymbol{k}'$) are incoming (outgoing) momenta for nucleons and DM particle, respectively (the index i refers to the ith nucleon).

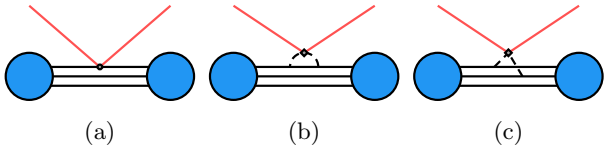

FIG. 1: (Color online): diagrams contributing to DM-nucleus scattering up to NLO. Solid black lines denote nucleons, dashed denote pions. Left panel: interaction at LO. Middle panel: one-body interaction at NLO. Right panel: two-body interaction at NLO.

In momentum space, the one body current describing the DM interaction with the ith nucleon up to NLO can be written as [11, 32]

$$\begin{aligned} J^{(1)}(\boldsymbol{q}_i) = {} & \frac{c_{\text{is}}}{\tilde{\Lambda}^3}\left[\sigma_{\pi N} - \frac{9 g_A^2 \pi m_\pi^3}{4(4\pi f_\pi)^2} F\left(\frac{|\boldsymbol{q}_i|}{2m_\pi}\right)\right] \\ & - \frac{c_{\text{iv}}}{\tilde{\Lambda}^3}\frac{\delta m_N}{4}\tau_i^z + \frac{c_s}{\tilde{\Lambda}^3}\left(\sigma_s - \dot{\sigma}_s \boldsymbol{q}^2\right) - \frac{c_G}{\tilde{\Lambda}^3}\frac{8\pi m_N^G}{9} \\ F(x) = {} & \frac{-x + (1+2x^2)\arctan x}{3x}, \end{aligned} \tag{4}$$

where $\sigma_{\pi N}$ is the nucleon σ-term, $\delta m_N = (m_n - m_p)_{\text{strong}}$, $\sigma_s = m_s \langle N|\bar{s}s|N\rangle$, $m_N^G = m_N - \sigma_{\pi N} - \sigma_s$, and $\dot{\sigma}_s = (0.3 \pm 0.2)\text{GeV}^{-2}$ [33]. Moreover, we defined the isoscalar and isovector couplings $c_{\text{is,iv}}$ as the appropriate linear combinations of the Wilson coefficients appearing in Eq. (2)

$$c_{\text{is}} = \frac{c_u m_u + c_d m_d}{m_u + m_d}, \tag{5}$$

$$c_{\text{iv}} = 2\frac{c_d m_d - c_u m_u}{m_d - m_u}. \tag{6}$$

The numerical values for the single-nucleon quantities used in calculations are taken from [34] and [35], i.e.:

$$\sigma_{\pi N} = (59.1 \pm 3.5)\ \text{MeV}, \quad \delta m_N = (2.32 \pm 0.17)\ \text{MeV}. \tag{7}$$

Even though we use the value for the $\sigma-$term obtained from a Roy-Steiner analysis of pion-nucleon scattering in [34], our numerical results can be easily extended to other values coming, for example, from lattice-QCD calculations (see [36] and references therein).

As noted in Section IV, the $\sigma-$term is factored out of the cross section so the numerical input used will only affect the relative size of the momentum dependent part of the one-body current.

The two-body current appearing at NLO (Fig. 1c), is given by

$$J^{(2)}_{\pi\pi}(\boldsymbol{q}_i, \boldsymbol{q}_j) = -\frac{c_{\text{is}}}{\tilde{\Lambda}^3}\left(\frac{g_A}{2F_\pi}\right)^2 m_\pi^2 \boldsymbol{\tau}_i\cdot\boldsymbol{\tau}_j \frac{\boldsymbol{\sigma}_i\cdot\boldsymbol{q}_i \boldsymbol{\sigma}_j\cdot\boldsymbol{q}_j}{(\boldsymbol{q}_i^2 + m_\pi^2)(\boldsymbol{q}_j^2 + m_\pi^2)}. \tag{8}$$

The coordinate-space expressions of the currents are provided in the Appendix. Two-nucleon currents proportional to c_G appear formally at N3LO [7, 11, 32].

The elastic scattering cross section is given by

$$\frac{d\sigma}{d\boldsymbol{q}^2} = \frac{1}{4\pi v_\chi^2}\frac{1}{2j+1} \times \sum_{m_j,m_j'=-j}^{j} \left|\langle\psi_{jm_j'}|J(\boldsymbol{q})|\psi_{jm_j}\rangle\right|^2 , \tag{9}$$

where v_χ is the velocity of the DM particle and we are adopting nonrelativistic states normalization for the DM particle and nucleus. The nuclear matrix element for a given nucleus with ground state $|\psi_{jm_j}\rangle$ is characterized by total spin j and spin polarization m_j and is calculated using $J(\boldsymbol{q})$, given by the sum of one- and two-body contributions from Eq. (4) and Eq. (8)

III. NUCLEAR WAVE FUNCTIONS

The evaluation of nuclear matrix elements required in Eq. (9) is performed using the Variational Monte Carlo method. We use variational wave functions $|\psi\rangle$ that minimize the expectation value of

$$E_V = \frac{\langle\psi|H|\psi\rangle}{\langle\psi|\psi\rangle} , \tag{10}$$

which provides an upper bound to the energy of the ground state.

The phenomenological Hamiltonian used in this work has an Argonne v_{18} potential [21] for the two-body interaction and Urbana IX [22] for the three-body:

$$H = \sum_i T_i + \sum_{i<j} v_{ij} + \sum_{i<j<k} v_{ijk} . \tag{11}$$

The variational wave function for a given nucleus in the J state is:

$$|\psi\rangle = \left[\mathcal{S}\prod_{i<j}^{A}(1+U_{ij})\right]\left[\prod_{i<j<k} f_c(r_{ijk})\right]|\Phi(JMTT_3)\rangle , \tag{12}$$

where $\mathcal{S}$ is a symmetrization operator acting on two- and three-body correlation operators, f_c is a spin- and isospin-independent two- and three-body correlation, Φ is an antisymmetric wave function containing the correct quantum numbers for the state of interest, and the two-body spin- and isospin-dependent correlations are constructed as

$$U_{ij} = \sum_p f^p(r_{ij})O_{ij}^p , \tag{13}$$

where the operators are

$$O_{ij}^p = \boldsymbol{\tau}_i\cdot\boldsymbol{\tau}_j, \boldsymbol{\sigma}_i\cdot\boldsymbol{\sigma}_j, (\boldsymbol{\tau}_i\cdot\boldsymbol{\tau}_j)(\boldsymbol{\sigma}_i\cdot\boldsymbol{\sigma}_j), S_{ij}, S_{ij}\boldsymbol{\tau}_i\cdot\boldsymbol{\tau}_j, \tag{14}$$

and f^p are radial functions. For more details see [23] and references therein.

Finally, the currents entering Eq. (9) are given by

$$J(\boldsymbol{q}) = \sum_i e^{i\boldsymbol{q}\cdot\boldsymbol{r}_i}J^{(1)}(\boldsymbol{q}) + \sum_{i<j} J^{(2)}_{\pi\pi}(\boldsymbol{q};\boldsymbol{r}_i,\boldsymbol{r}_j) , \tag{15}$$

obtained by Fourier transforming the expressions in Eq. (4) and Eq. (8), as reported in Appendix.

IV. RESULTS

Here we present the results of our calculations, for a variety of light nuclei. Considering for the moment only the isoscalar part (the contribution of $c_{\rm iv}$, c_s and c_G is easily included according to Eq. (17) below), it is convenient, as in [11], to expand the total cross section in terms of nuclear response functions

$$\frac{d\sigma}{d\boldsymbol{q}^2} = \frac{c_{\rm is}^2}{\tilde{\Lambda}^6}\frac{\sigma_{\pi N}^2 A^2}{4\pi v_\chi^2}\left|\mathcal{F}^{(0)}_{\rm is}(\boldsymbol{q}^2) + \mathcal{F}^{(1)}_{\rm is,2b}(\boldsymbol{q}^2) + \mathcal{F}^{(1)}_{\rm is,r}(\boldsymbol{q}^2)\right|^2 , \tag{16}$$

where we factorized the isoscalar coupling, σ-term and the number of nucleons A. Each function $\mathcal{F}^{(\nu)}_{a,i}$ carries an index ν referring to the chiral order, labels a to distinguish between isoscalar and isovector contributions, i for contributions of two-body currents and for the so-called "nucleon radius" correction, given by the one-body momentum-dependent correction in Eq. (4) proportional to $F\left(\frac{|\boldsymbol{q}_i|}{2m_\pi}\right)$. With our choice of normalization, we have $\mathcal{F}^{(0)}_{\rm is}(0) = 1$.

In what follows we concentrate on the case $c_{\rm is} \neq 0$ while setting $c_{\rm iv,s,G}/c_{\rm is} = 0$, because to the order we work the additional couplings do not introduce independent nuclear responses. In fact, from Eq. (4) one can obtain the cross section for general couplings $c_{\rm iv,s,G} \neq 0$ by rescaling $\mathcal{F}^{(0)}_{\rm is}(\boldsymbol{q}^2)$ in Eq. (16) by the factor

$$1 - \left(\frac{c_{\rm iv}}{c_{\rm is}}\right)\frac{\delta m_N}{4\sigma_{\pi N}}\frac{2Z-A}{A} + \left(\frac{c_{\rm s}}{c_{\rm is}}\right)\frac{\sigma_s - \dot{\sigma}_s\,\boldsymbol{q}^2}{\sigma_{\pi N}} - \left(\frac{c_G}{c_{\rm is}}\right)\frac{8\pi m_N^G}{9\sigma_{\pi N}} . \tag{17}$$

The maximum momentum transfer q considered in the calculations is 100 MeV, which is appropriate for light nuclei and DM mass of about 1 GeV. In this scenario q ranges from a few to tens of MeV. In Fig. 2 we present the results for isoscalar terms in Eq. (16). For each nucleus, we compare the results for LO and NLO contributions. As we can see, the order ($\nu = 1$) corrections slightly increase the cross section at low momenta. At larger momenta, the contribution from the radius correction is greater than the two-body and of opposite sign, making the total cross section decrease as q increases. This behavior is consistent for all the nuclei considered

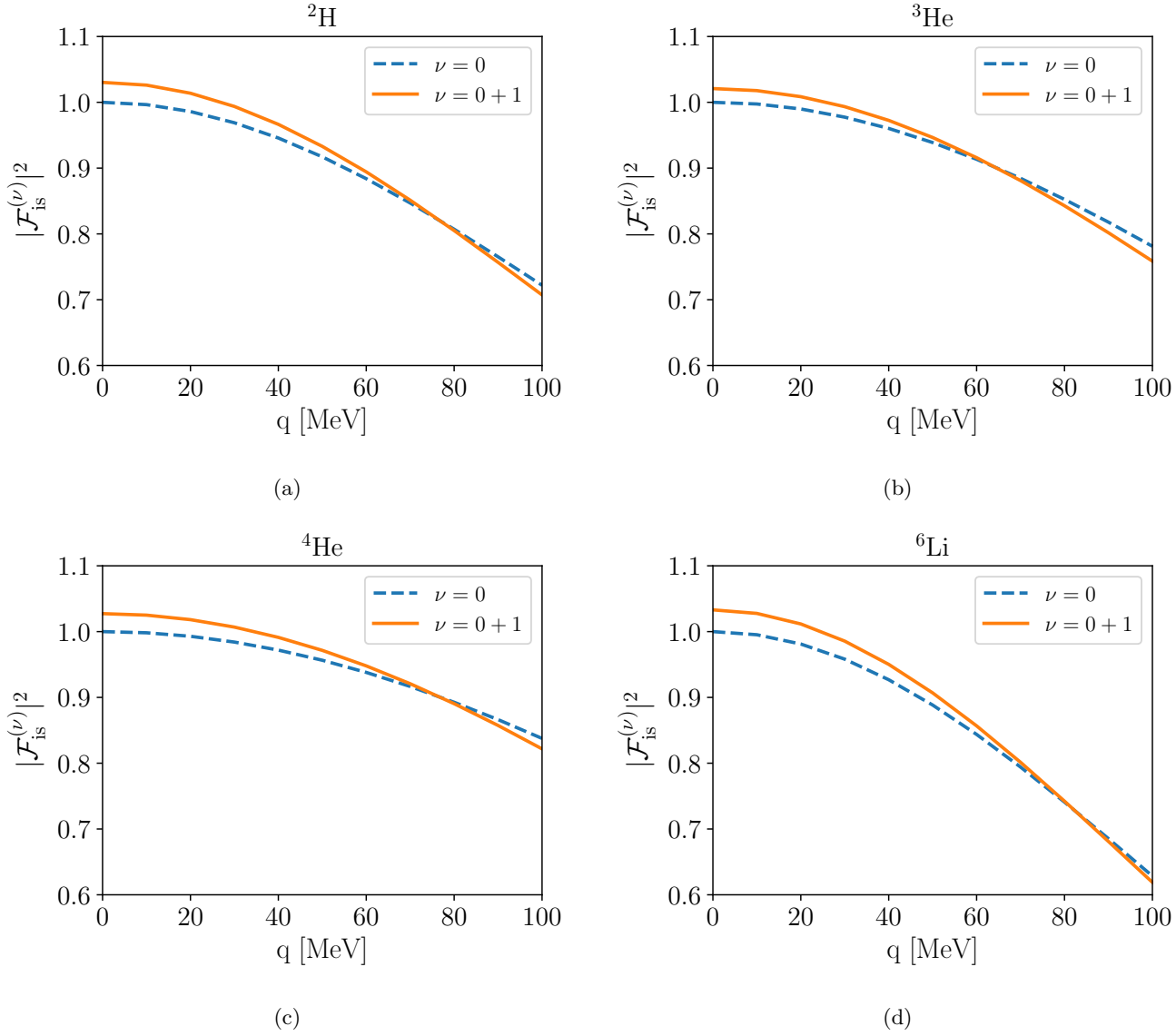

FIG. 2: (color online) Isoscalar matrix elements for nuclei from A=2 to 6. Dashed blue lines correspond to LO calculations, and orange solid ones to NLO.

here. Nonetheless, in the range of values considered, the deviation from LO results is at the few percent level.

In order to assess the effect of the two terms appearing at order ($\nu = 1$), it is useful to consider their relative contribution to the total cross section. First, we define the radius correction in the following way [11]

$$\Delta^{(r)} = \frac{|\mathcal{F}_{\rm is}^{(0+1)}(\boldsymbol{q}^2)|^2 - |\mathcal{F}_{\rm is}^{(0)}(\boldsymbol{q}^2) + \mathcal{F}_{\rm is,2b}^{(1)}(\boldsymbol{q}^2)|^2}{|\mathcal{F}_{\rm is}^{(0+1)}(\boldsymbol{q}^2)|^2}\,, \quad (18)$$

where $\mathcal{F}_{\rm is}^{(0+1)}(\boldsymbol{q}^2)$ is defined by the sum of the three isoscalar terms on the right-hand side of Eq. (16). Working at NLO and expanding for small order ($\nu = 1$) corrections, this expression reduces to

$$\Delta^{(r)} \sim \frac{2\mathcal{F}_{\rm is,r}^{(1)}(\boldsymbol{q}^2)}{\mathcal{F}_{\rm is}^{(0+1)}(\boldsymbol{q}^2)} \sim -\frac{2}{\sigma_{\pi N}} \frac{9g_A^2\pi m_\pi^3}{4(4\pi f_\pi)^2} F\left(\frac{|\boldsymbol{q}|}{2m_\pi}\right). \quad (19)$$

The nuclear effects drop out and the correction is given only by the momentum-dependence of Eq. (4). This expression agrees with the complete nuclear calculations, in the range of the momenta considered here. For this reason, we only present the radius correction for ^{4}He in Fig. 3, and note that all the other nuclei show the same behavior, up to minor differences due to the two-body contribution and higher order terms in the expansion (19). The radius correction vanishes at zero momentum transfer and grows to about 6% at $q = 100$ MeV.

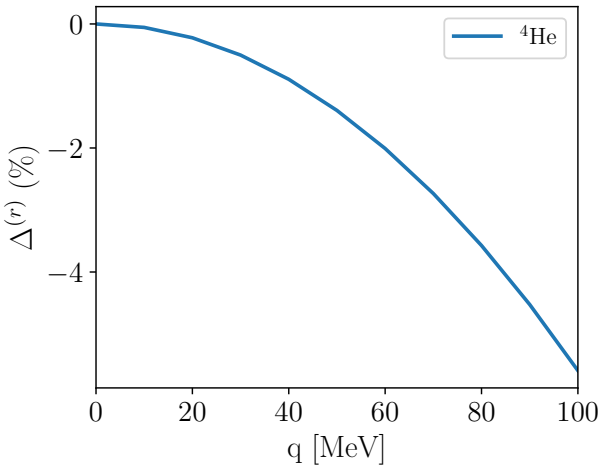

FIG. 3: Percentual radius correction for ^{4}He

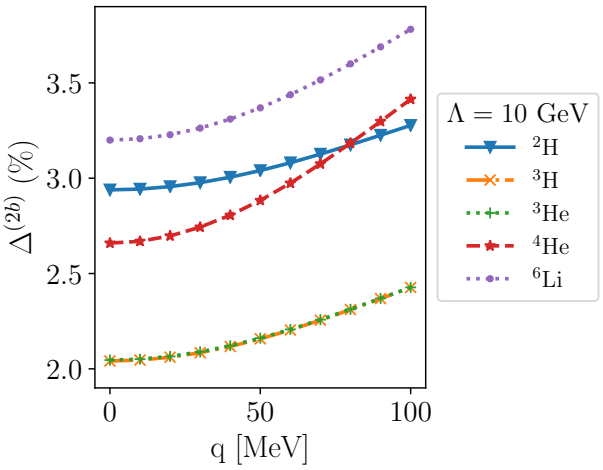

FIG. 4: (color online) Percentual two-body correction to total cross section for various nuclei.

Similarly to Eq. (18), the relative contribution of two body currents is given by [11]

$$\Delta^{(2b)} = \frac{\left|\mathcal{F}_{\rm is}^{(0+1)}(\boldsymbol{q}^2)\right|^2 - \left|\mathcal{F}_{\rm is}^{(0)}(\boldsymbol{q}^2) + \mathcal{F}_{\rm is,r}^{(1)}(\boldsymbol{q}^2)\right|^2}{\left|\mathcal{F}_{\rm is}^{(0+1)}(\boldsymbol{q}^2)\right|^2}. \quad (20)$$

In Fig. 4 we present the percentual correction given by two-body operators entering at NLO with respect to the total contribution up to NLO. All two-body corrections are of modest size, with nuclei with $A = 3$ giving a smaller contribution compared to ^{2}H and ^{4}He, and being almost exactly equal. The two-body corrections tend to increase with the nucleus size at large momenta and this effect might be even more pronounced for larger nuclei. We notice however that al low momenta the correction in ^{2}H nucleus is somehow larger than A=3 and 4 nuclei. Overall, the role of two-body operators increases with the momentum transferred, from about 2% up to about 4%. This is true only for very large cutoff and note, however, that the actual size of the correction depends on our choice $c_{\rm iv,s,G} = 0$, and can be computed in the general case through the rescaling introduced in Eq. (17) above. Also, radius and two-body corrections for different values of the nucleon $\sigma-$term can be obtained from our data multiplying by the appropriate constant. Lower values of the $\sigma-$term as in [36] increase the relative size of NLO contributions.

Finally, we discuss the cutoff-dependence of the nuclear matrix elements due to the short-distance regulator introduced in the Fourier transforms (see Appendix). All the results reported so far were obtained in the limit of infinite cutoff Λ in Eq. (23). Ideally, one should consider a cutoff in the current consistent to the one used in the nuclear Hamiltonian, but this is not possible in our hybrid approach. In fact, since we use a phenomenological potential in the nuclear Hamiltonian, there are no "strong" low energy constant that allow for a variation of the cutoff when obtaining the nuclear wave function. In practice, since the Argonne v_{18} interaction has a very strong hard core, we might expect its effective cutoff to be very high. In such situations, a possible strategy would be to fix the cutoff in the currents, fit the "weak" low-energy constants to reproduce some observable, and predict properties of larger nuclei. For Argonne Hamiltonians this has been for example explored in β-decay calculations [29]. However, in the present case, up to the order we work, there are no new low-energy constants in the currents and this approach is not viable. So to explore the cutoff dependence we have simply calculated $\Delta^{(2b)}$ for different values of Λ. The calculations are presented in Fig. 4 and Fig. 5 where we show the fractional two-body corrections at $\Lambda = 500$ MeV and $\Lambda = 10$ GeV,

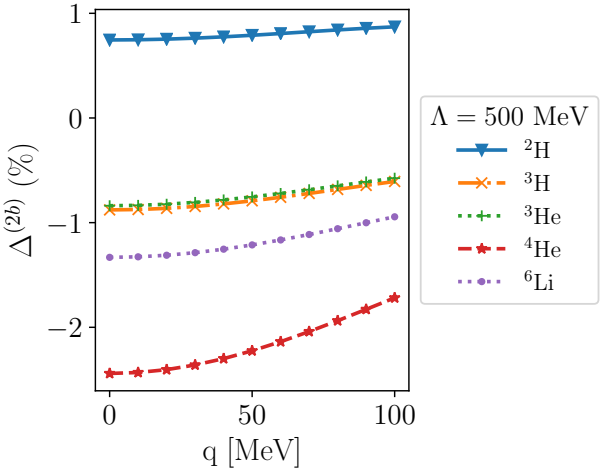

FIG. 5: (color online) Percentual two-body correction to total cross section for various nuclei.

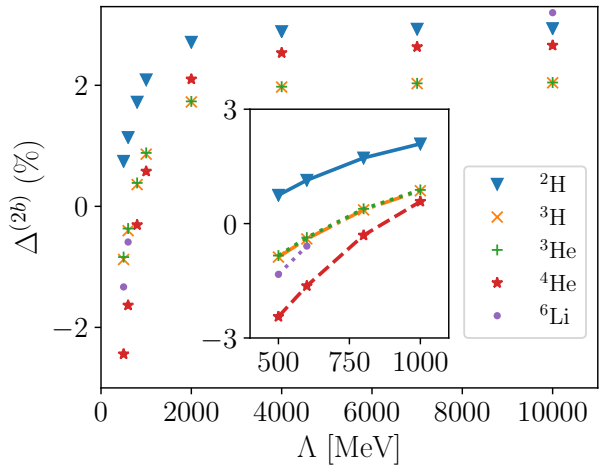

FIG. 6: Cutoff dependence of the two-body contribution for $q = 0$.

respectively, as a function of q. In Fig. 6 we show the two-body corrections for all the nuclei considered here as a function of the cutoff Λ for a fixed $q = 0$.

Nucl.	Λ [MeV]	$\Delta^{(2b)}$ (%)		
		$\mathcal{O}_1$	$\mathcal{O}_2$	$\mathcal{O}_1 + \mathcal{O}_2$
^{2}H	500	-3.4	4.2	0.7
	10000	-4.9	7.9	3.0
^{4}He	500	-13.2	10.7	-2.4
	10000	-19.2	21.9	2.7

TABLE I: Percentual two-body correction to total cross section for nonvanishing operators contributing at $q = 0$.

Two features emerge from our results. First, for $\Lambda \in [500, 1000]$ MeV there is a strong cutoff dependence of the two-body contribution, so that it even changes signs for some nuclei. For example, the two-body correction is always positive for ^{2}H, but it changes sign in A=3 nuclei and ^{6}Li for $\Lambda \sim 700$ MeV and above 800 MeV for ^{4}He. This is due to the fact that there is a large cancellation between the operators in Eq. (23). We illustrate this point by reporting in Table I the fractional contributions to the total cross section at q=0, which arise entirely from the operators $\mathcal{O}_1$ ($\sim \boldsymbol{\sigma}_1 \cdot \boldsymbol{\sigma}_2$) and $\mathcal{O}_2$ ($\sim \boldsymbol{\sigma}_1 \cdot \hat{\boldsymbol{r}}\, \boldsymbol{\sigma}_2 \cdot \hat{\boldsymbol{r}}$) in Eq. (23). The second feature is that the two-body contribution saturates for large values of Λ, starting around 2 GeV. This might reflect the fact that the phenomenological nuclear Hamiltonian considered here effectively has a very large cutoff. Overall, the cutoff dependence of the two-body current contribution is the largest source of uncertainty in our approach. Attempts to remove this "systematic" effect will necessarily involve the use of wave functions obtained by a chiral potential, as discussed in Ref. [11].

V. CONCLUSIONS

We have studied the elastic scattering of DM particles off a number of light nuclei (^{2}H, ^{3}H, ^{3}He, ^{4}He and ^{6}Li) with different spin and isospin using Quantum Monte Carlo Methods. We have focused on scalar-mediated interactions, parametrized by four Wilson coefficients related to the mediator mass and its coupling to DM and quarks. We have used the resulting hadronic currents up to NLO in the chiral expansion, containing both nucleon "scalar radius" corrections and two-body effects. We have followed a hybrid approach in which the chiral EFT currents are used in combination with nuclear wave functions obtained from a phenomenological nuclear Hamiltonian that includes the Argonne v_{18} two-body interaction, and the three-body Urbana IX.

We find that for the momentum transfers of interest, the overall size of the NLO corrections is at the few % level, perhaps smaller than suggested by chiral counting. The NLO correction due to nucleon scalar radius is essentially free of nuclear structure uncertainties and grows from zero to $\approx -2\%$ at $q = 60$ MeV and $\approx -6\%$ at $q = 100$ MeV. On the other hand, the corrections due to scalar two-body currents — estimated for $A = 4, 6$ for the first time in this work — start at $q = 0$ at the 2–3% level (depending on the nucleus) and mildly grow with q. For $A = 2, 3$, our results are in qualitative agreement with [11].

We can also compare our findings for ^{3}He and ^{4}He with Ref. [30]. This reference considers only the one-body current, generated by the operator $\hat{\mathcal{O}}_1$ in the NREFT operator basis of Ref. [5]. While a detailed numerical comparison is beyond the scope of our work, for the one-body contribution we find a good qualitative agreement with the results of Ref. [30].

Even assigning a conservative uncertainty as large as the variation of the two-body matrix element between $\Lambda = 500$ MeV and $\Lambda = 2$ GeV, the total cross-section is still known quite precisely, namely at the few % level. Therefore, our results in combination with Refs. [11, 30] already provide reasonable nuclear structure input needed to assess the sensitivity of future experimental searches of light dark matter using ^{3}He and ^{4}He targets.

Further refinements are certainly warranted. Interesting directions for future studies include: (i) moving beyond the hybrid approach, in the spirit of Ref. [11], by using chiral interactions (as opposed to the Argonne v_{18} potential) in combination with Quantum Monte Carlo to obtain the nuclear wave functions; (ii) exploring the consistency of Weinberg power counting in various channels of DM-nucleon two-body interactions, and matching to lattice-QCD calculations [13, 14], to determine the relevant low energy constants

Acknowledgments

We thank J. Carlson, W. Detmold, D. Lonardoni, E. Mereghetti, S. Pastore, R. Schiavilla and J. de Vries for discussions and correspondence. V.C. acknowledges support by the US DOE Office of Nuclear Physics and by the LDRD program at Los Alamos National Laboratory. The work of S.G. was supported by the NUCLEI SciDAC program, by the U.S. DOE under contract DE-AC52-06NA25396, by the LANL LDRD program, and by the DOE Early Career Research Program. Computational resources have been also provided by Los Alamos Institutional Computing, and we also used resources provided by NERSC, which is supported by the US DOE under Contract DE-AC02-05CH11231.

VI. APPENDIX

The one- and two body DM-nucleon currents need to be Fourier transformed so that they can be used in a Variational Monte Carlo calculation in coordinate space. To tame the short-distance singularities we use a Gaussian regulator of the form

$$S_\Lambda(\boldsymbol{k}^2) = e^{-\frac{\boldsymbol{k}^2}{2\Lambda^2}} \ , \tag{21}$$

with cutoff parameter Λ. The two-body current is obtained from

$$J^{(2)}_{\pi\pi}(\boldsymbol{q};\boldsymbol{r}_1,\boldsymbol{r}_2) = \int \frac{d^3\boldsymbol{k}_1}{(2\pi)^3}\frac{d^3\boldsymbol{k}_2}{(2\pi)^3} e^{i\boldsymbol{k}_1\cdot\boldsymbol{r}_1} e^{i\boldsymbol{k}_2\cdot\boldsymbol{r}_2} S_\Lambda(\boldsymbol{k}_1^2) S_\Lambda(\boldsymbol{k}_2^2) \times (2\pi)^3\delta^{(3)}(\boldsymbol{k}_1+\boldsymbol{k}_2-\boldsymbol{q}) J^{(2)}_{\pi\pi}(\boldsymbol{k}_1,\boldsymbol{k}_2) \tag{22}$$

The coordinate space expression for two-body currents can be calculated analytically, except for one integration over an auxiliary variable y. It reads

$$\begin{aligned} J^{(2)}_{\pi\pi}(\boldsymbol{q};\boldsymbol{r}_1,\boldsymbol{r}_2) = &-\frac{1}{\Lambda^3}\left(\frac{g_A}{2F_\pi}\right)^2 c_{\rm is} m_\pi^2 \boldsymbol{\tau}_1\cdot\boldsymbol{\tau}_2 \times \\ &\frac{1}{2} e^{i\boldsymbol{q}\cdot\boldsymbol{R}} \int_{-1}^{1} dy e^{-i\boldsymbol{q}\cdot\boldsymbol{r}y/2} \times \Bigg[\\ &(\boldsymbol{\sigma}_1\cdot\boldsymbol{q})(\boldsymbol{\sigma}_2\cdot\boldsymbol{q})\frac{1-y^2}{4} s(r,y) + \\ &(\boldsymbol{\sigma}_1\cdot\boldsymbol{q})(\boldsymbol{\sigma}_2\cdot\hat{\boldsymbol{r}})\left(-i\frac{1+y}{2}\right)\frac{\partial}{\partial r} s(r,y) + \\ &(\boldsymbol{\sigma}_1\cdot\hat{\boldsymbol{r}})(\boldsymbol{\sigma}_2\cdot\boldsymbol{q})\left(i\frac{1-y}{2}\right)\frac{\partial}{\partial r} s(r,y) + \\ &(\boldsymbol{\sigma}_1\cdot\boldsymbol{\sigma}_2)\frac{1}{r}\frac{\partial}{\partial r} s(r,y) + \\ &(\boldsymbol{\sigma}_1\cdot\hat{\boldsymbol{r}})(\boldsymbol{\sigma}_2\cdot\hat{\boldsymbol{r}}) r \frac{\partial}{\partial r}\frac{1}{r}\frac{\partial}{\partial r} s(r,y) \Bigg], \end{aligned} \tag{23}$$

where $\boldsymbol{r} = \boldsymbol{r}_2 - \boldsymbol{r}_1$, $\boldsymbol{R} = \frac{\boldsymbol{r}_2+\boldsymbol{r}_1}{2}$ and the radial functions have the following expressions:

$$s(r,y) = \frac{e^{L^2/\Lambda^2}}{8\pi L\Lambda r}\left[\operatorname{erfc}\left(\frac{L}{\Lambda}+\frac{\Lambda r}{2}\right)e^{Lr}\left(\frac{L}{\Lambda}+\frac{\Lambda r}{2}\right) - \operatorname{erfc}\left(\frac{L}{\Lambda}-\frac{\Lambda r}{2}\right)e^{-Lr}\left(\frac{L}{\Lambda}-\frac{\Lambda r}{2}\right)\right] \tag{24}$$

$$\frac{\partial}{\partial r}s(r,y) = \frac{e^{L^2/\Lambda^2}}{8\pi\Lambda^2 r^2}\left[\operatorname{erfc}\left(\frac{L}{\Lambda}+\frac{\Lambda r}{2}\right)e^{Lr}\left(-1+Lr+\frac{\Lambda^2 r^2}{2}\right) + \operatorname{erfc}\left(\frac{L}{\Lambda}-\frac{\Lambda r}{2}\right)e^{-Lr}\left(1+Lr-\frac{\Lambda^2 r^2}{2}\right)\right] - \frac{e^{-\Lambda^2 r^2/4}}{4\pi^{3/2}\Lambda r} \tag{25}$$

$$r\frac{\partial}{\partial r}\frac{1}{r}\frac{\partial}{\partial r}s(r,y) = \frac{e^{L^2/\Lambda^2}}{8\pi\Lambda^2 r^3}\left[\operatorname{erfc}\left(\frac{L}{\Lambda}+\frac{\Lambda r}{2}\right)e^{Lr}\left(3-3Lr+L^2r^2-\frac{\Lambda^2 r^2}{2}+\frac{Lr\Lambda^2 r^2}{2}\right) + \operatorname{erfc}\left(\frac{L}{\Lambda}-\frac{\Lambda r}{2}\right)e^{-Lr}\left(-3-3Lr-L^2r^2+\frac{\Lambda^2 r^2}{2}+\frac{Lr\Lambda^2 r^2}{2}\right)\right] + \frac{3e^{-\Lambda^2 r^2/4}}{4\pi^{3/2}\Lambda r^2} \tag{26}$$

$$r^2\frac{\partial}{\partial r}\frac{1}{r}\frac{\partial}{\partial r}\frac{1}{r}\frac{\partial}{\partial r}s(r,y) = \frac{e^{L^2/\Lambda^2}}{8\pi\Lambda^2 r^4}\left[\operatorname{erfc}\left(\frac{L}{\Lambda}+\frac{\Lambda r}{2}\right)e^{Lr}\left(-10+10Lr-5L^2r^2+L^3r^3-Lr\Lambda^2 r^2+\frac{L^2r^2\Lambda^2 r^2}{2}\right) + \operatorname{erfc}\left(\frac{L}{\Lambda}-\frac{\Lambda r}{2}\right)e^{-Lr}\left(10+10Lr+5L^2r^2+L^3r^3-Lr\Lambda^2 r^2-\frac{L^2r^2\Lambda^2 r^2}{2}\right)\right] - \frac{e^{-\Lambda^2 r^2/4}(10+L^2r^2+\Lambda^2 r^2)}{4\pi^{3/2}\Lambda r^3} \tag{27}$$

$$L(\boldsymbol{q};y) = \sqrt{m^2+(1-y^2)\frac{\boldsymbol{q}^2}{4}} \tag{28}$$

As a useful cross-check, we can see that in the limit of $q = 0$ and $\Lambda \to \infty$ the above expression reduces to

$$\frac{1}{8\pi r}\left[(\boldsymbol{\sigma}_1\cdot\hat{\boldsymbol{r}})(\boldsymbol{\sigma}_2\cdot\hat{\boldsymbol{r}})(1+mr)-(\boldsymbol{\sigma}_1\cdot\boldsymbol{\sigma}_2)\right]e^{-mr}\ , \tag{29}$$

which corresponds to Eq. (5.8) and (5.9) in [7].

[1] G. Bertone and D. Hooper, Submitted to: Rev. Mod. Phys. (2016), arXiv:1605.04909 [astro-ph.CO].
[2] M. Battaglieri et al., (2017), arXiv:1707.04591 [hep-ph].
[3] J. Engel, S. Pittel, and P. Vogel, Int. J. Mod. Phys. **E1**, 1 (1992).
[4] J. Fan, M. Reece, and L.-T. Wang, JCAP **1011**, 042 (2010), arXiv:1008.1591 [hep-ph].
[5] A. L. Fitzpatrick, W. Haxton, E. Katz, N. Lubbers, and Y. Xu, JCAP **1302**, 004 (2013), arXiv:1203.3542 [hep-ph].
[6] G. Prezeau, A. Kurylov, M. Kamionkowski, and P. Vogel, Phys. Rev. Lett. **91**, 231301 (2003), arXiv:astro-ph/0309115 [astro-ph].
[7] V. Cirigliano, M. L. Graesser, and G. Ovanesyan, Journal of High Energy Physics **2012**, 25 (2012).
[8] J. Menendez, D. Gazit, and A. Schwenk, Phys. Rev. **D86**, 103511 (2012), arXiv:1208.1094 [astro-ph.CO].
[9] M. Hoferichter, P. Klos, and A. Schwenk, Phys. Lett. **B746**, 410 (2015), arXiv:1503.04811 [hep-ph].
[10] M. Hoferichter, P. Klos, J. Menéndez, and A. Schwenk, Phys. Rev. D **94**, 063505 (2016).
[11] C. Körber, A. Nogga, and J. de Vries, Phys. Rev. C **96**, 035805 (2017).
[12] F. Bishara, J. Brod, B. Grinstein, and J. Zupan, JHEP **11**, 059 (2017), arXiv:1707.06998 [hep-ph].
[13] E. Chang, Z. Davoudi, W. Detmold, A. S. Gambhir, K. Orginos, M. J. Savage, P. E. Shanahan, M. L. Wagman, and F. Winter (NPLQCD Collaboration), Phys. Rev. Lett. **120**, 152002 (2018).
[14] S. R. Beane, S. D. Cohen, W. Detmold, H. W. Lin, and M. J. Savage, Phys. Rev. **D89**, 074505 (2014), arXiv:1306.6939 [hep-ph].
[15] W. Guo and D. N. McKinsey, Phys. Rev. **D87**, 115001 (2013), arXiv:1302.0534 [astro-ph.IM].
[16] T. M. Ito and G. M. Seidel, Phys. Rev. **C88**, 025805 (2013), arXiv:1303.3858 [astro-ph.IM].
[17] G. Gerbier et al., (2014), arXiv:1401.7902 [astro-ph.IM].
[18] S. Profumo, Phys. Rev. **D93**, 055036 (2016),

arXiv:1507.07531 [hep-ph].
[19] S. A. Hertel, A. Biekert, J. Lin, V. Velan, and D. N. McKinsey, (2018), arXiv:1810.06283 [physics.ins-det].
[20] F. Mayet et al., Phys. Rept. **627**, 1 (2016), arXiv:1602.03781 [astro-ph.CO].
[21] R. B. Wiringa, V. G. J. Stoks, and R. Schiavilla, Phys. Rev. C **51**, 38 (1995).
[22] B. S. Pudliner, V. R. Pandharipande, J. Carlson, S. C. Pieper, and R. B. Wiringa, Phys. Rev. C **56**, 1720 (1997).
[23] J. Carlson, S. Gandolfi, F. Pederiva, S. C. Pieper, R. Schiavilla, K. E. Schmidt, and R. B. Wiringa, Rev. Mod. Phys. **87**, 1067 (2015).
[24] J. E. Lynn, I. Tews, J. Carlson, S. Gandolfi, A. Gezerlis, K. E. Schmidt, and A. Schwenk, Phys. Rev. Lett. **116**, 062501 (2016).
[25] D. Lonardoni, J. Carlson, S. Gandolfi, J. E. Lynn, K. E. Schmidt, A. Schwenk, and X. B. Wang, Phys. Rev. Lett. **120**, 122502 (2018).
[26] A. Lovato, S. Gandolfi, R. Butler, J. Carlson, E. Lusk, S. C. Pieper, and R. Schiavilla, Phys. Rev. Lett. **111**, 092501 (2013).
[27] A. Lovato, S. Gandolfi, J. Carlson, S. C. Pieper, and R. Schiavilla, Phys. Rev. Lett. **117**, 082501 (2016).
[28] A. Lovato, S. Gandolfi, J. Carlson, S. C. Pieper, and R. Schiavilla, Phys. Rev. Lett. **112**, 182502 (2014).
[29] S. Pastore, A. Baroni, J. Carlson, S. Gandolfi, S. C. Pieper, R. Schiavilla, and R. B. Wiringa, Phys. Rev. C **97**, 022501 (2018).
[30] D. Gazda, R. Catena, and C. Forssn, Phys. Rev. **D95**, 103011 (2017), arXiv:1612.09165 [hep-ph].
[31] F. Bishara, J. Brod, B. Grinstein, and J. Zupan, Journal of Cosmology and Astroparticle Physics **2017**, 009 (2017).
[32] A. Crivellin, M. Hoferichter, and M. Procura, Phys. Rev. **D89**, 054021 (2014), arXiv:1312.4951 [hep-ph].
[33] M. Hoferichter, C. Ditsche, B. Kubis, and U. G. Meissner, JHEP **06**, 063 (2012), arXiv:1204.6251 [hep-ph].
[34] M. Hoferichter, J. Ruiz de Elvira, B. Kubis, and U.-G. Meißner, Phys. Rev. Lett. **115**, 092301 (2015).
[35] D. A. Brantley, B. Joo, E. V. Mastropas, E. Mereghetti, H. Monge-Camacho, B. C. Tiburzi, and A. Walker-Loud, (2016), arXiv:1612.07733 [hep-lat].
[36] P. E. Shanahan, J. Phys. **G43**, 124001 (2016), arXiv:1606.08812 [hep-lat].